

Journal of Materials Chemistry A

Accepted Manuscript



This is an *Accepted Manuscript*, which has been through the Royal Society of Chemistry peer review process and has been accepted for publication.

Accepted Manuscripts are published online shortly after acceptance, before technical editing, formatting and proof reading. Using this free service, authors can make their results available to the community, in citable form, before we publish the edited article. We will replace this *Accepted Manuscript* with the edited and formatted *Advance Article* as soon as it is available.

You can find more information about *Accepted Manuscripts* in the [Information for Authors](#).

Please note that technical editing may introduce minor changes to the text and/or graphics, which may alter content. The journal's standard [Terms & Conditions](#) and the [Ethical guidelines](#) still apply. In no event shall the Royal Society of Chemistry be held responsible for any errors or omissions in this *Accepted Manuscript* or any consequences arising from the use of any information it contains.

**A simple in situ tubular chemical vapor deposition processing of
large-scale efficient perovskite solar cells and the research on its
novel roll-over phenomenon in J-V curve**

Paifeng Luo^{a*} Zhaofan Liu^a Wei Xia^a Chenchen Yuan^b Jigui Cheng^a
Yingwei Lu^a

*^aDepartment of Materials Science and Engineering, Hefei University of Technology,
Hefei, Anhui 230009, P.R. China*

*^bCAS Key Laboratory of Materials for Energy Conversion, University of Science and
Technology of China, Hefei, Anhui 230026, P.R. China*

*corresponding author: Paifeng Luo

E-mail: lpfeng@hfut.edu.cn or lpfeng@mail.ustc.edu.cn

Tel: +86-551-62904566

Fax: +86-551-62905285

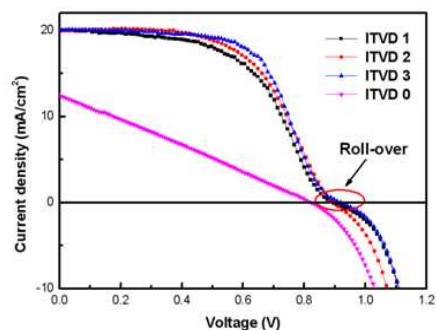
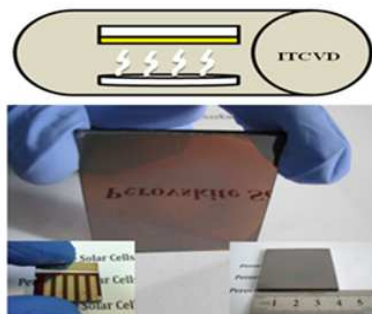
* Correspondent: Paifeng Luo
E-mail: lpfeng@hfut.edu.cn or lpfeng@mail.ustc.edu.cn
Tel: +86-551-62904566 Fax: +86-551-62905285

Abstract

Hybrid perovskite solar cells (PSCs) with excellent photoelectric properties have attracted tremendous attention in recent years. However, current thermal evaporation technology and solution-based route are still challenging to produce low-cost, large-scale, and uniform perovskite absorbers. Herein, we present a simple in situ tubular chemical vapor deposition (ITCVD) method to fabricate perovskite films. And initial results on the demonstrated sample with a size of 4cm×4cm show potential of large area deposition by ITCVD. Meanwhile, the prepared $\text{CH}_3\text{NH}_3\text{PbI}_3$ films have an orthorhombic perovskite structure, and exhibit a high crystallinity, and show outstanding optical properties. Accordingly, high efficiency of 12.2% is also successfully achieved based on our first batch of planar type PSCs. More intriguingly, the novel roll over phenomenon in J-V curve of PSCs is first investigated in this study, and further research proves that it is caused by the recently discovered $\text{PbI}_2/\text{CH}_3\text{NH}_3\text{PbI}_3$ heterojunction, which can help us to further understand the fundamental working mechanism of PSCs.

Key words: Perovskite solar cells; In situ tubular vapor deposition; High crystallinity; Roll over phenomenon; $\text{PbI}_2/\text{CH}_3\text{NH}_3\text{PbI}_3$ heterojunction

Table of Content (TOC):



1. Introduction

Nowadays, hybrid inorganic-organic perovskite compounds with large absorption, suitable band gap and long-range carrier diffusion length, have been regarded as one of the most promising materials for solar energy conversion[1-8]. Generally, the hybrid perovskite is represented by a simple building block AMX_3 , where A is the organic cation, M and X is the metal cation and halide anion, respectively. In 2009, Miyasaka firstly applied the hybrid perovskite as light sensitizer into the dye-sensitized solar cells (DSCs) and achieved an efficiency of 3.8%[9]. Subsequently, perovskite materials were widely used as the light harvester in quantum dot (QD), solid-state mesoscopic and planar heterojunction solar cells[10-14]. Quite recently, PSCs have reached the astonishing high efficiency of 19.3% and attracted unprecedented attention in PV field[15].

To date, most of the PSCs are dominantly prepared by the thermal evaporation method and the solution spin-coating route[14-20]. But vacuum-based technology requires expensive equipment and complicated process, which is not an ideal cost-efficient way to deposit uniform, large-scale perovskite films. On the other side, the most studied solution method has a cost advantage, but always results in rough film surface and incomplete coverage. To avoid shunting current, compact and nonporous films must be obtained during the preparing process of perovskite PV device, especially for the planar-type heterojunction configuration. Therefore, development of a low-cost, large-scale, and effective deposition technology has been considered as an urgent demand for the practical applications of PSCs.

Recently, vapor-assisted solution process (VASP) was exploited and demonstrated as an effective route for preparing uniform perovskite films. But VASP

need processed in the glove box, and the complicated manipulations hinder its further large-scale applications[21]. Very recently, low-pressure chemical vapor deposition (LPCVD) and hybrid CVD (HCVD) were developed to prepare high efficient PSCs by our group and Qi, respectively[4,6]. It is well known that CVD approaches can deposit uniform films in large area and have been widely employed as cost-efficient methods to produce all kinds of semiconductor materials. However, both of the LPCVD and HCVD are equipped with double heating zones, and need the gas diffusion or transport process from one zone to the other. So it requires accurate control of the vacuum pressure or carrier gas flow, and also demands prevention of the condensation of $\text{CH}_3\text{NH}_3\text{I}$ vapor, which will tremendously affect the reproducibility and is also difficult to realize the controllable preparation of PSCs.

Herein, to take advantages of the vapor-assisted process and CVD methods, a simple in situ tubular chemical vapor deposition (ITCVD) technology is developed to fabricate perovskite absorbers. Our method offers several advantages: Without the need of a glove box and/or vacuum instruments[14,17,22], the most applied tubular furnace is employed to grow perovskite films, which should be a cost-effective way to fabricate PSCs and shows the potential for large area deposition. Meanwhile, only reaction temperature and time are required to be considered in the single zone ITCVD. Thus our method is much more controllable than those of LPCVD and HCVD approaches as mentioned above. As a result, large perovskite films with a size of $4\text{cm}\times 4\text{cm}$ are demonstrated by our simple method. It is found that the prepared films exhibit high quality and excellent optical properties through X-ray diffraction(XRD), Raman, scanning electron microscope(SEM), absorption spectroscopy and photoluminescence (PL) measurements. Finally, PSCs with high efficiency of 12.2% are successfully obtained in this work. More strikingly, a novel roll over phenomenon

in J-V curve is also first investigated. The impedance spectroscopy (IS), Capacitance-voltage (C-V) measurements and XPS measurements, demonstrate that the observed “roll-over” in the JV curve is due to the presence of $\text{PbI}_2/\text{CH}_3\text{NH}_3\text{PbI}_3$ heterojunction in PSCs.

2. Experimental

2.1. Fabrication of PSCs: Fig.1 shows the schematic diagram of preparation of PSCs. Firstly, the compact- TiO_2 films were obtained by spin-coating the Titanium isopropoxide/HCl solution on the etched FTO-coated glass and sintering at $500\text{ }^\circ\text{C}$ for

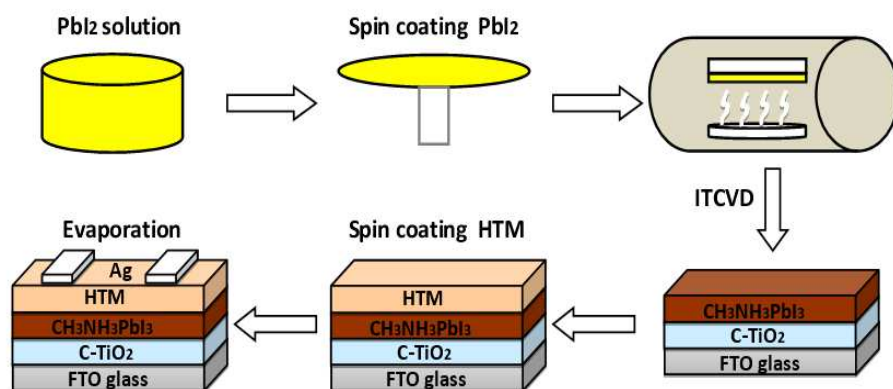


Fig. 1. The schematic diagram of preparation of PSCs.

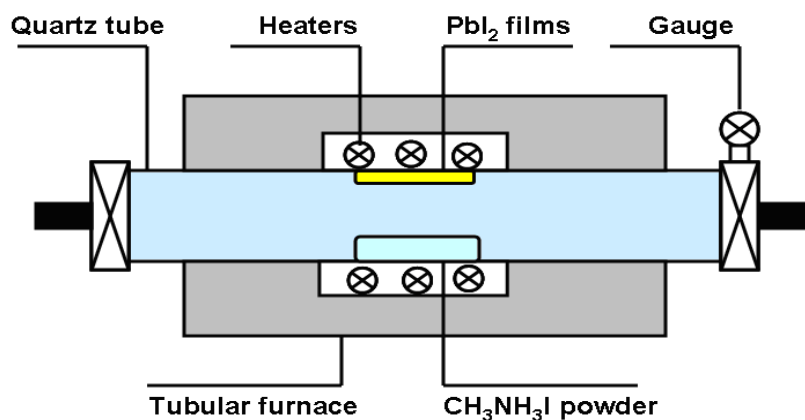


Fig. 2. The schematic diagram of in situ chemical vapor deposition (ITCVD) equipment.

30min. Secondly, $\text{CH}_3\text{NH}_3\text{I}$ was synthesized by the reaction of methylamine and hydroiodic acid as the recipe of Yang[21]. PbI_2 films were prepared by spin-coating the N,N -dimethylformamide(DMF)/ PbI_2 solution at a concentration of 400mg/mL. The obtained PbI_2 films were placed on the right above $\text{CH}_3\text{NH}_3\text{I}$ powder, as shown in Fig.2, and the whole tube is heated to 145 °C and reacted for 120min. Then, the reacted films were washed with isopropanol and annealed at 145 °C for 30min in air. Thirdly, the hole-transporting material was deposited by spin coating at 4000 rpm for 30 s and the solution was synthesized by dissolving 72.3 mg spiro-MeOTAD, 17.5 μL of lithium bis(trifluoromethanesulfonyl)imide solution (520mg LITSEI in 1mL acetonitrile) and 28.8 μL 4-tert-butylpyridine in 1mL chlorobenzene. Finally, silver or gold electrode was deposited by thermal evaporation with a stainless steel mask (active area: 0.12cm²).

2.2. Characterizations: The phase composition and the crystal structure were identified by XRD method (D/MAX2500V). Raman spectroscopy was measured by a Focal Laser MicroRaman Spectrometer (LABRAM-HR) with an excitation 514.5nm. The morphology and composition were observed by field emission scanning electron microscope (FESEM, Sirion200). The absorption spectrum was recorded by UV-visible spectrophotometer (CARY 5000) with the wavelength range of 300nm~1000nm. Steady-state photoluminescence (PL) was analyzed using Steady-state lifetime Spectrofluorometer (FIUOROLOG-3-TAU) with an exciting wavelength of 370 nm and detection at 770nm. The current density-voltage (J-V) curves were measured with a Keithley 2400 source meter under illumination of 100mW/cm², AM1.5 by a solar simulator (Newport, Oriel Sol3A 94023A) in air. The step voltage was fixed at 10mV and the active area of single cells is 0.12cm². EQE was measured with a Newport EQE measurement kit(IQE-200) by focusing the

monochromatic beam of light onto the devices. The electrochemical impedance measurement was carried out under different forward bias of 0.6 V, 0.7V and 0.8V in the dark using an electrochemical workstation (CHI660C) from 1 Hz to 100 kHz. The magnitude of the alternative signal was 5mV. Capacitance-voltage (C-V) measurement was performed at different fixed frequencies of 10Hz, 1 kHz, 2 kHz and 10 kHz in the dark. X-ray photoemission spectroscopy (XPS) was carried out on a VG ESCALAB250 surface analysis system equipped with a monochromatic Al X-ray (1486.6 eV) source.

3. Results and discussion

Fig.3 shows the X-ray diffraction patterns of coated PbI_2 films and $\text{CH}_3\text{NH}_3\text{PbI}_3$. From the XRD, it can be observed that PbI_2 films with hexagonal structure show a high peak at 12.64° , and have a strong preferred (001) orientation. After ITCVD process, deducting the diffractions of $\text{TiO}_2/\text{FTO}/\text{Glass}$ substrate, $\text{CH}_3\text{NH}_3\text{PbI}_3$ films with a preferred (110) orientation shows an orthorhombic crystal structure. And the peaks at 14.17° , 28.38° , 31.87° , and 43.17° assign to the (110), (220), (310) and (330) planes, respectively. From the graph, all the peaks of $\text{CH}_3\text{NH}_3\text{PbI}_3$ in the XRD are

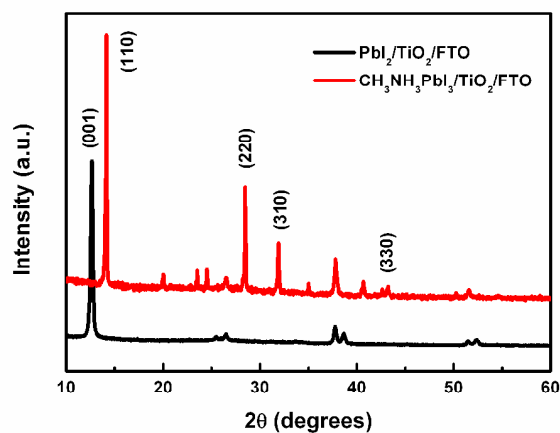


Fig. 3. The XRD of coated PbI_2 films (black line) and $\text{CH}_3\text{NH}_3\text{PbI}_3$ absorbers (red line).

well accord with the reported plots[21], and all the diffractions of PbI_2 are disappeared and fully converted into perovskite structure. Generally, the intercalating reaction between the inorganic PbI_2 and the organic $\text{CH}_3\text{NH}_3\text{I}$ is so quick and usually results in rough surface and porous films, especially for the solution based route[23]. But during the ITCVD process, the dilute $\text{CH}_3\text{NH}_3\text{I}$ vapor can slowly penetrate into the layered PbI_2 films and effectively reduce the intercalating rate. So the ITCVD method is expected to obtain uniform and full covered perovskite films.

Generally, AMX_3 perovskite materials have three structures named orthorhombic, tetragonal and cubic phases. In order to accurately characterize the structure of $\text{CH}_3\text{NH}_3\text{PbI}_3$ films, Raman spectra are performed using LABRAM-HR spectrometer. Fig.4 shows the Raman spectrum of $\text{CH}_3\text{NH}_3\text{PbI}_3$ absorbers. And there are strong peaks at 94cm^{-1} , 143cm^{-1} , 209cm^{-1} and 339cm^{-1} in the wavenumber range of 80-500 cm^{-1} . The band at 94cm^{-1} is assigned to the bending and stretching of Pb-I bonds, which is the diagnostic mode of the inorganic cages. And the broad unstructured $200\sim 400\text{cm}^{-1}$ feature is assigned to the torsional mode of methylammonium cations[24]. At present, there is still some controversy about the crystal structure of

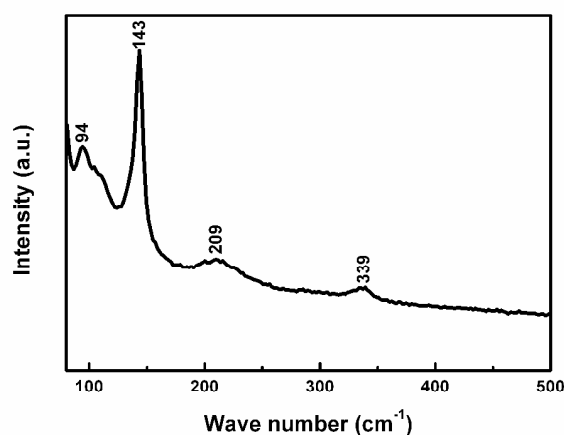


Fig. 4. The Raman spectra of $\text{CH}_3\text{NH}_3\text{PbI}_3$ absorbers.

$\text{CH}_3\text{NH}_3\text{PbI}_3$ films which belongs to the orthorhombic phase or tetragonal phase. Maalej has systematically studied the phase transition and crystal dynamics in $\text{CH}_3\text{NH}_3\text{PbCl}_3$ and demonstrated the characteristic peaks of different crystal structures[25]. Herein, our plots show the strong peaks at low wavenumber range, especially the strong peak at 143cm^{-1} , which is well accord with the characteristic peak of the orthorhombic crystal structure[26].

The morphology of $\text{CH}_3\text{NH}_3\text{PbI}_3$ films is very crucial for the planar-type perovskite solar cells. The rough and incomplete covered film surface usually reported in the solution route will lead to the shunting current and deteriorate the device performance[23]. Fig. 5(a) and (b) shows the SEM of $\text{CH}_3\text{NH}_3\text{PbI}_3$ absorbers. From the low- and high-magnification SEM, the dense, well-defined uniform grains with large size that attained submicron levels are obtained, and the as-formed perovskite films demonstrate the characteristics of full surface coverage on the $\text{TiO}_2/\text{FTO}/\text{Glass}$ substrate. As a demonstration for proving the scalability of our process, a large sample with a structure of $\text{CH}_3\text{NH}_3\text{PbI}_3/\text{TiO}_2/\text{FTO}/\text{Glass}$, as shown in Fig.6 (a), is also successfully prepared by ITCVD method. The demonstrated dark brown sample with a big size of $4\text{cm}\times 4\text{cm}$ exhibits smooth morphology over a relatively large area. For detect the uniformity, middle point A and edge point B,

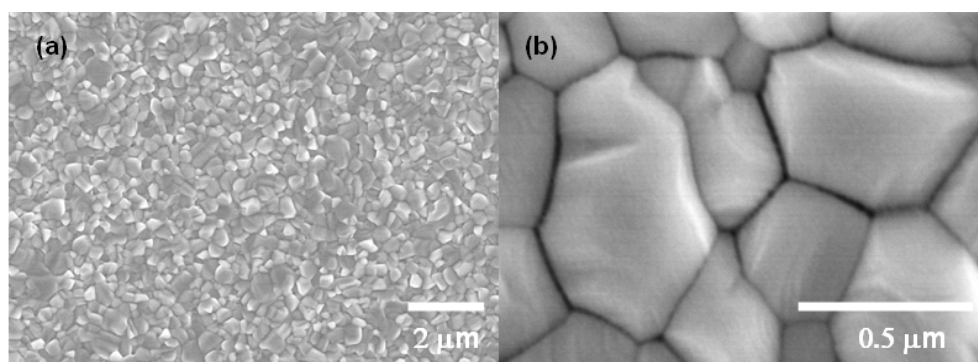


Fig. 5. The (a) low- and (b) high-magnification SEM of $\text{CH}_3\text{NH}_3\text{PbI}_3$ absorbers.

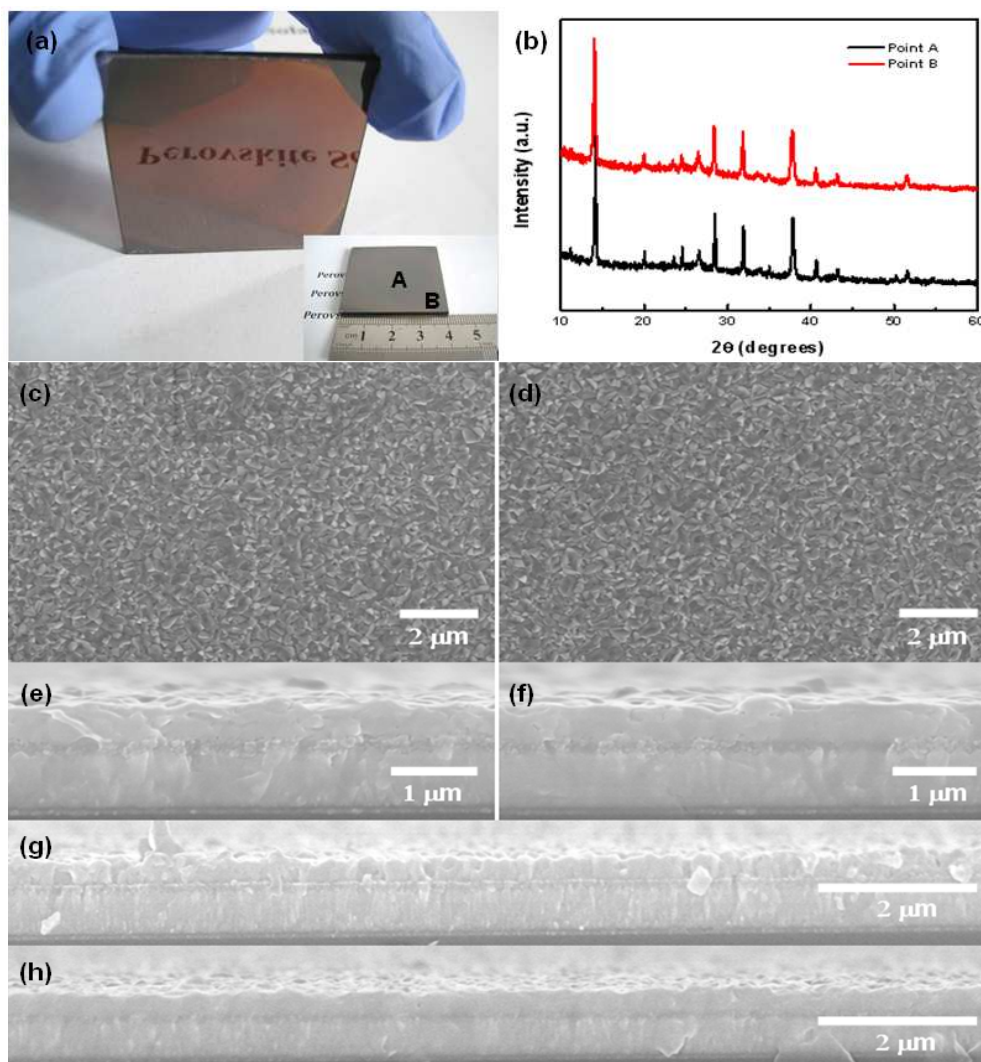


Fig. 6. (a) The photographs of the big demonstrated sample with a size of 4cm×4cm; (b) XRD patterns of points A and B; (c), (e), and (g) Planar, high-magnification cross-sectional, low-magnification cross-sectional SEM images of point A, respectively; (d), (f), and (h) Planar, high-magnification cross-sectional, low-magnification cross-sectional SEM images of point B, respectively.

based on the symmetry of our sample, are investigated by XRD and low- and high-magnification SEM shown in Fig. 6 (b), (c), (d), (e), (f), (g), and (h), respectively. As mentioned above, the $\text{CH}_3\text{NH}_3\text{I}$ vapor molecule slowly penetrates into the porous PbI_2 films, and the compact, uniform $\text{CH}_3\text{NH}_3\text{PbI}_3$ films are obtained through the typical intercalating reaction, as shown in Fig. 6. Thus our simple ITCVD method can

easily produce the large-scale, high-quality perovskite films, which is also very suitable for the fabrication of planar-type PSCs.

The optical properties of $\text{CH}_3\text{NH}_3\text{PbI}_3$ absorbers are characterized by the absorption spectrum and steady-state photoluminescence (PL), respectively. As shown in Fig. 7(a), the $\text{CH}_3\text{NH}_3\text{PbI}_3$ films have an optical absorption at around 770nm, which is consistent with the reported spectrum[27,28]. The absorption edge is also very sharp, which indicates a direct band gap. This is in good agreement with the theoretical calculations, where all the electronic structure models predict a direct band gap for the Sn- and Pb- analogues[27,29]. Our films demonstrate a broad absorption range covering the whole visible range (400-800nm) with a high absorption coefficient above $6 \times 10^4 \text{cm}^{-1}$ based on 320nm film thickness. The PL of $\text{CH}_3\text{NH}_3\text{PbI}_3$ films is also shown in Fig. 7(a). An intense PL emission at 775nm is observed, and it is right at the band edge only with a little Stokes-shift. So the PL emission wavelength is accord with the optical absorption spectrum and supplies further evidence for the feature of direct band gap. According to the calculating formula of the direct band gap materials: $\alpha(h\nu) = A(h\nu - E_g)^{1/2}$, where $h\nu$ is photon energy and A is an arbitrary constant, a band gap (E_g) of 1.55eV is deduced by plotting the graph between $(\alpha h\nu)^2$

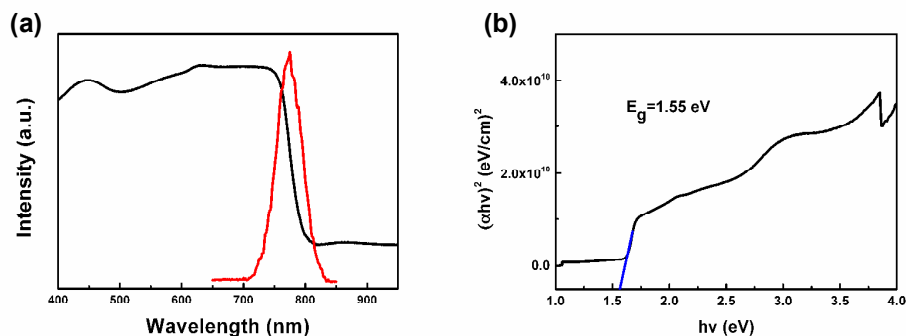


Fig. 7(a) The absorption spectrum and steady-state photoluminescence (PL); (b) the $(\alpha h\nu)^2$ against $h\nu$ of optical absorption spectra of $\text{CH}_3\text{NH}_3\text{PbI}_3$ films.

vs $h\nu$, as shown in Fig. 7(b). In brief, the obtained $\text{CH}_3\text{NH}_3\text{PbI}_3$ films by ITCVD process are the ideal light harvester candidate for the preparation of PSCs.

Fig.8 shows (a) the photograph and (b) the cross-sectional SEM of the fabricated PSCs. From the cross-sectional SEM, we can clearly observe top Ag electrode, spiro-OMeTAD layer, $\text{CH}_3\text{NH}_3\text{PbI}_3$ absorbers, compact- TiO_2 layer and FTO glass. The thickness of $\text{CH}_3\text{NH}_3\text{PbI}_3$ absorbers is about 320nm, while FTO glass is partly etched by HCl and Zn powder during the preparing process of PSCs. As a result, a high efficiency of 12.2% is successfully achieved based on our first batch of the planar-type PSCs. Fig. 9(a) shows the J-V curves of the best efficient PSCs and its dark current. Intriguingly, the device shows a crossover of the J-V curve and the dark current curve at the voltages slightly moves above the V_{oc} . The external quantum efficiency (EQE) spectrum of the best device is also shown in Fig. 9(b). A wide response in the range of 400-800 nm can be observed, indicating full absorption and efficient carrier extraction in the PSCs. We detected four pieces of PSCs and the photovoltaic performance is shown in Tab. 1. All the efficiencies of annealed devices are near and/or above 10%, which implies our ITCVD method can present efficient PSCs. More intriguingly, the novel roll over phenomenon in J-V curves of the best device in Fig. 9(a) and the rest three cells named ITCVD1, 2, and 3 in Fig. 9(c), is

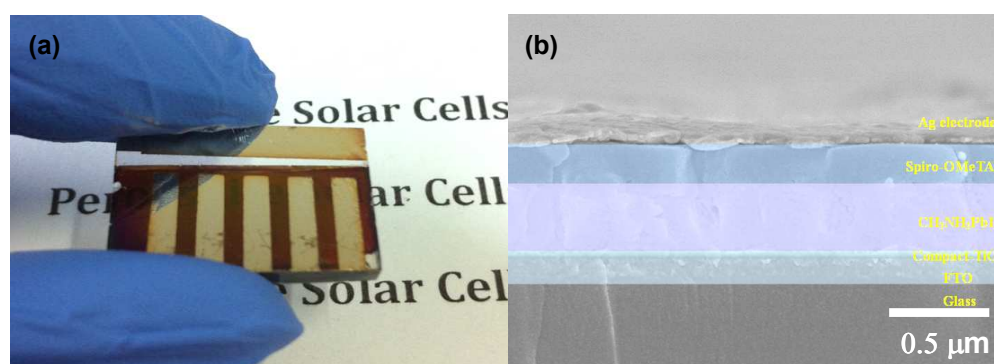


Fig. 8 (a) The photograph and (b) the cross-sectional SEM of PSCs.

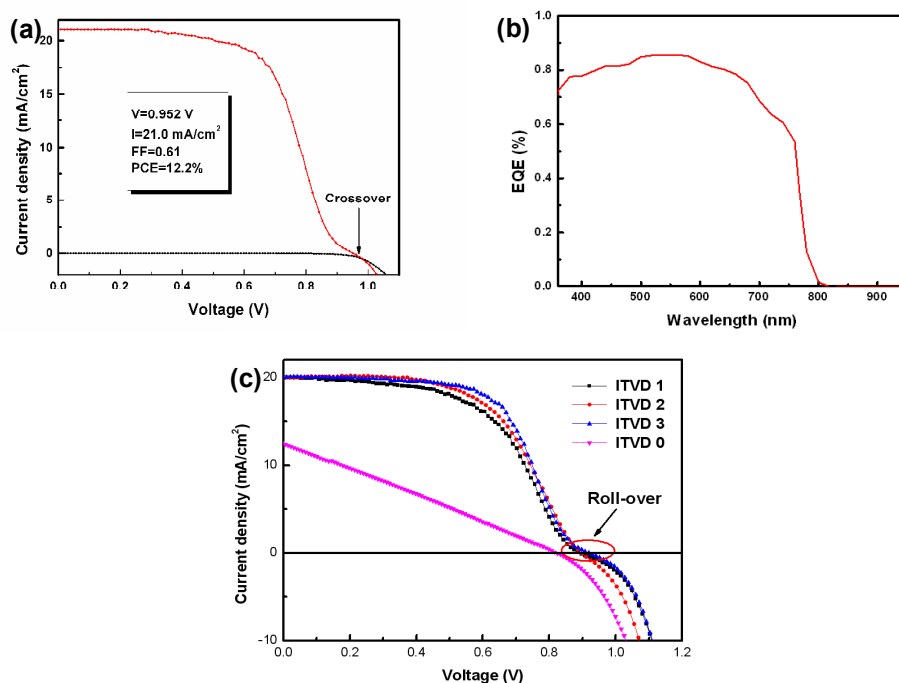


Fig. 9 (a) The J-V and dark current curves, and (b) the EQE of the best efficient PSCs ITCVD4; (c) the roll over J-V curves of the rest three PSCs ITCVD 1, 2, and 3, and the J-V curve of PSCs without annealing ITCVD 0.

Tab. 1. Performance data for perovskite solar cells.

Device No.	V_{oc} (V)	J_{sc} (mA cm^{-2})	FF	PCE(%)
ITCVD 0	0.825	12.50	0.26	2.68
ITCVD 1	0.892	20.06	0.55	9.84
ITCVD 2	0.895	20.10	0.57	10.3
ITCVD 3	0.920	20.09	0.60	11.1
ITCVD 4	0.952	21.00	0.61	12.2

first reported in PSCs. From the previous vapor-assisted and CVD work, we can clearly observe the roll over phenomenon but no one notice this special characteristic[4,6,21,30]. Only Yang reported the crossover and roll over behaviors of CIGS thin-film solar cells and attributed to the acceptor-like defects at the

interface[31]. Our previous work also proves that the presence of PbI_2 can passivate the grain boundaries and enhance the performance of PSCs[4]. As a comparison, we examined the PV performance of PSCs without annealing treatment, and its J-V curve is also shown in Fig. 9(c). The poor efficiency of 2.68% is due to the presence of a large amount of charge traps in perovskite films, and there is no roll over characteristic in its J-V curve.

In Fig. 10 (a), comparing with the patterns without annealing, the signals of PbI_2 are clearly observed in the films annealed for 30min, which has been reported by other groups[30,32-34]. So here we speculate that this special J-V characteristic is resulted from the presence of PbI_2 in $\text{CH}_3\text{NH}_3\text{PbI}_3$ absorbers. Yang claims that PbI_2 is located in grain boundaries (GBs) of perovskite absorbers[30]. But how it works since the carrier transport direction is perpendicular to the direction of built-in electric field? So we speculate that the decomposition during the annealing process mostly occurs on

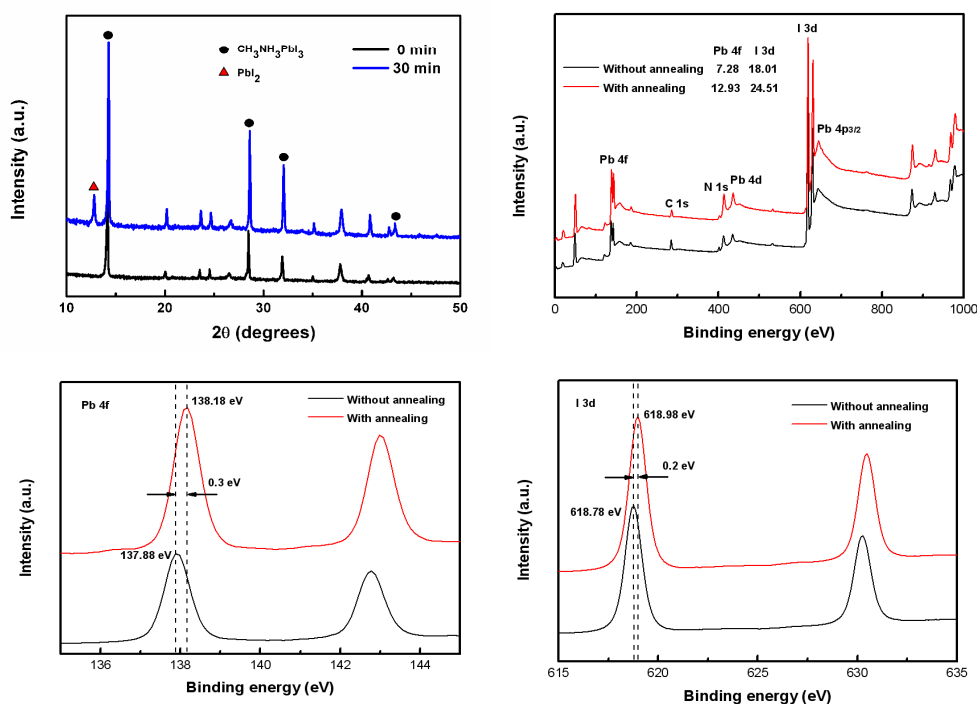


Fig. 10 (a) XRD of $\text{CH}_3\text{NH}_3\text{PbI}_3$ films with different annealing time; (b) Overall, Pb4f, and I3d XPS spectra of perovskite films with and without annealing, respectively.

the surface of $\text{CH}_3\text{NH}_3\text{PbI}_3$ films since the surface layer is very easy to decompose. Fig. 10(b), (c), and (d) shows the overall, Pb4f, and I3d XPS spectra of perovskite films with and without annealing, respectively. All the signals of C1s, N1s, Pb4f, Pb4P3/2, I3d appear in both of the two films. And the banding energies shift 0.3eV with Pb4f and 0.2eV with I3d core levels, which is in good agreement with Lindlad's results[35]. It is also found that the ratio of I3d and Pb4f changes from 2.5 to 1.9 after annealing, which means the surface $\text{CH}_3\text{NH}_3\text{PbI}_3$ films decompose to PbI_2 .

In order to further investigate the effect of surface PbI_2 on its charge transfer mechanism of PSCs, the IS based on a simple and straightforward structure of $\text{Au}/\text{CH}_3\text{NH}_3\text{PbI}_3/\text{TiO}_2/\text{FTO}/\text{Glass}$ is employed in this study. In order to focus on the $\text{PbI}_2/\text{CH}_3\text{NH}_3\text{PbI}_3$ interface, HTM layer is not included in this structure here. Nyquist plots over the frequency range of 100Hz to 10kHz in the dark are obtained in Fig. 11(a). Different forward applied voltages (V_{app}) are used to simulate the actual light illumination operation condition. Except the curve of 0.8V V_{app} , all the spectra present an arc at high frequencies (low Z'), which is attributed to the charge transfer resistance at the gold back contact[36,37]. While the transmission line (TL) patterns with a straight line followed by the arc are also observed. This phenomenon unequivocally shows the carrier transport coupled with recombination along the entire active thickness. Generally, the TL feature only appears when carrier diffusion length (L_d) is larger than film thickness (L), which also indicates our PSCs have a long L_d and efficient charge transfer[36]. When L_d less than L at the higher V_{app} of 0.8V, TL pattern disappeared. Comparing with one arc situation of $\text{CH}_3\text{NH}_3\text{PbI}_3/\text{TiO}_2$ junction, we infer that there should have another charge transfer resistance coming from the presence of PbI_2 [38].

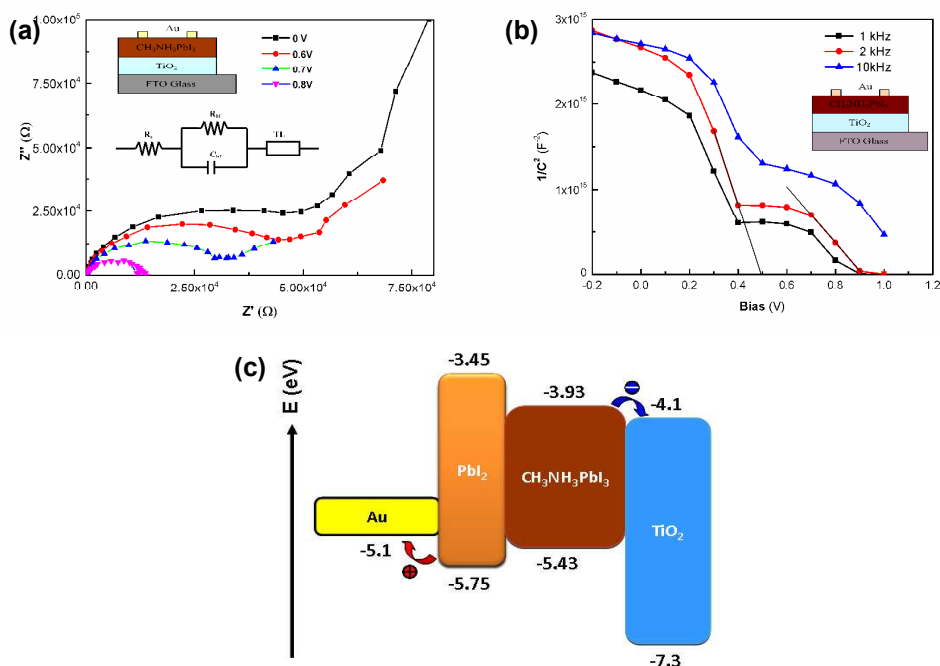


Fig.11 (a) Nyquist plot at different applied voltages and the series resistor (R_s), relevant high frequency resistance (R_{hf}), and capacitance (C_{hf}) are shown in the equivalent circuit model; (b) Mott-Schottky plots at different frequencies; (c) the proposed band energy alignment of the Au/CH₃NH₃PbI₃/TiO₂/FTO/Glass device.

Thus the C-V measurement is also employed to explore more useful information about the carrier transport characteristics. Mott-Schottky plots under 1kHz, 2kHz and 10kHz are shown in Fig. 11(b). Apparently, capacitance decreases with the increasing frequency, which implies a contribution to the junction space charge from relatively slow deep levels. Basically, the built-in potential (V_{bi}) can be deduced from the equation: $\frac{1}{C^2} = \frac{2}{q\epsilon\epsilon_0 A^2 N} (V_{bi} - V)$, where N is the carrier density, A is the active area, ϵ is the static permittivity, ϵ_0 is the permittivity of free space, q is the elementary charge. Thus the carrier density is calculated to be $9.32 \times 10^{16} \text{cm}^{-3}$ by fitting the slope of C^{-2} vs V at 2kHz[39,40]. Strikingly, during the forward bias range, there are two linear regions of the C^{-2} vs V plots, and the intercepts of straight lines at 2kHz yield

0.91V and 0.49V, respectively. The bigger value of 0.91V undoubtedly assigns to the V_{bi} of $\text{CH}_3\text{NH}_3\text{PbI}_3/\text{TiO}_2$ p-n junction, which is in well agreement with the predicted theoretical V_{oc} of PSCs. In terms of the presence of PbI_2 on the surface of $\text{CH}_3\text{NH}_3\text{PbI}_3$ films and their conduction band offsets $\Delta E_c = 0.48\text{eV}$, we infer that the smaller value of 0.49V is possibly ascribed to the undiscovered $\text{PbI}_2/\text{CH}_3\text{NH}_3\text{PbI}_3$ heterojunction. Thus the relevant band energy alignment is also proposed in Fig. 11(c), in which the main recombination between electrons and holes near the gold back electrode is blocked by the high energy barrier of PbI_2 . And the observed ΔE_c can be served as a back surface field and assists the extraction of electrons. Therefore, it can be concluded that the presence of PbI_2 is mostly located on the surface, but not in the GBs, and forms $\text{PbI}_2/\text{CH}_3\text{NH}_3\text{PbI}_3$ heterojunction paralleled to the electric field. So our findings are helpful to further understand the fundamental working mechanism of PSCs.

4. Conclusions

In brief, a simple and cost-efficient ITCVD method is firstly developed to fabricate PSCs in this study. As a result, a large perovskite sample with a size of $4\text{cm} \times 4\text{cm}$ is demonstrated by ITCVD. Meanwhile, the prepared $\text{CH}_3\text{NH}_3\text{PbI}_3$ absorbers with an orthorhombic perovskite structure have a high crystallinity, and demonstrate outstanding optical properties. As a consequence, PSCs fabricated without the need of a glove box present a high efficiency of 12.2%, which indicates a promising route for the future mass production. More intriguingly, the novel crossover and roll over behaviors in J-V curves are first investigated in PSCs, which is proven to be caused by the recently discovered $\text{PbI}_2/\text{CH}_3\text{NH}_3\text{PbI}_3$ heterojunction.

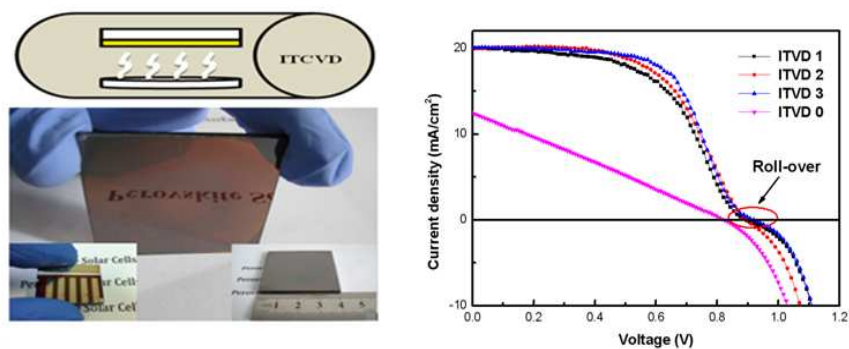
Acknowledgments

This work was financially supported by the National Natural Science Foundation of China (51302058) and the Opening Project of CAS Key Laboratory of Materials for Energy Conversion at University of Science and Technology of China (USTC).

References

1. M. M. Lee, J. Teuscher, T. Miyasaka, T. N. Murakami, H. J. Snaith, *Science*, 2012, **338**, 643-647.
2. J. Burschka, N. Pellet, S. -J. Moon, R. H. -Baker, P. Gao, M. K. Nazeeruddin, and M. Gratzel, *Nature*, 2013, **499**, 316-319.
3. S. D. Stranks, G. E. Eperon, G. Grancini, C. Menelaou, M. J. P. Alcocer, T. Leijtens, L. M. Herz, A. Petrozza, H. J. Snaith, *Science*, 2013, **342**, 341-344.
4. P. Luo, Z. Liu, W. Xia, C. Yuan, J. Cheng, and Y. Lu, *ACS Appl. Mater. Interfaces*, 2015, **7**, 2708-2714.
5. O. Malinkiewicz, A. Yella, Y. H. Lee, G. M. Espallargas, M. Gratzel, M. K. Nazeeruddin, and H. J. Bolink, *Nat. Photon.*, 2014, **8**, 128-132.
6. M. R. Leyden, L. K. Ono, S. R. Raga, Y. Kato, S. Wang, and Y. Qi, *J. Mater. Chem. A*, 2014, **2**, 18742-18745.
7. J. You, Y. Yang, Z. Hong, T. -B. Song, L. Meng, Y. Liu, C. Jiang, H. Zhou, W. -H. Chang, G. Li, and Y. Yang, *Appl. Phys. Lett.*, 2014, **105**, 183902.
8. J. A. Christians, R. C. Fung and P. V. Kamat, *J. Am. Chem. Soc.*, 2014, **136**, 758-764.
9. A. Kojima, K. Teshima, Y. Shirai, and T. Miyasaka, *J. Am. Chem. Soc.*, 2009, **131**, 6050-6051.
10. J. H. Im, C. Ryul. Lee, J. W. Lee, S. W. Park and N. G. Park, *Nanoscale*, 2011, **3**, 4088-4093.
11. H. S. Kim, C. R. Lee, J. H. Im, K. B. Lee, T. Moehl, A. Marchioro, S. J. Moon, R. H. Baker, J. H. Yum, J. E. Moser, M. Grätzel, N. G. Park, *Sci. Rep.*, 2012, **2**, 591-7.
12. J. M. Ball, M. M. Lee, A. Hey, H. J. Snaith, *Energy Environ. Sci.*, 2013, **6**, 1739-1743.
13. J. H. Noh, S. H. Im, J. H. Heo, T. N. Mandal, and S. I. Seok, *Nano Lett.*, 2013, **13**, 1764-1769.
14. M. Liu, M. B. Johnston & H. J. Snaith, *Nature*, 2013, **501**, 395-398.
15. H. Zhou, Q. Chen, G. Li, S. Luo, T. -B. Song, H. -S. Duan, Z. Hong, J. You, Y. Liu, Y. Yang, *Science*, 2014, **345**, 542-546.
16. Z. Cheng, and J. Lin, *CrystEngComm*, 2010, **12**, 2646-2662.
17. C. W. Chen, H. W. Kang, S. Y. Hsiao, P. F. Yang, K. M. Chiang, and H. W. Lin, *Adv. Mater.*, 2014, **26**, 6647-6652.
18. N. J. Jeon, J. H. Noh, Y. C. Kim, W. S. Yang, S. Ryu, and S. Seok, *Nat. Mater.*, 2014, **13**, 897-903.
19. D. Liu, and T. L. Kelly, *Nat. Photon.*, 2014, **8**, 133-138.

20. G. E. Eperon, V. M. Burlakov, P. Docampo, A. Goriely, and H. J. Snaith, *Adv. Funct. Mater.*, 2013, **24**, 151-157.
21. Q. Chen, H. Zhou, Z. Hong, S. Luo, H. -S. Duan, H. -H. Wang, Y. Liu, G. Li, and Y. Yang, *J. Am. Chem. Soc.*, 2014, **136**, 622-625.
22. H. Hu, D. Wang, Y. Zhou, J. Zhang, S. Lv, S. Pang, X. Chen, Z. Liu, N. P. Padture, G. Cui, *RSC Advances*, 2012, **00**, 1-3.
23. M. Xiao, F. Huang, W. Huang, Y. Dkhissi, Y. Zhu, J. Etheridge, A. G. -Weale, U. Bach, Y. -B. Cheng, and L. Spiccia, *Angew. Chem.*, 2014, **126**, 10056-10061.
24. C. Quarti, G. Grancini, E. Mosconi, P. Bruno, J. M. Ball, M. M. Lee, H. J. Snaith, A. Petrozza, and F. D. Angelis, *J. Phys. Chem. Lett.*, 2014, **5**, 279-284.
25. A. Maalej, O. Y. Abid, A. Kallel, O. A. Daoud, A. Lautie, and F. Romainb, *Solid State Commun*, 1997, **103**, 279-284.
26. S. Sasaki, C. T. Prewitt, J. D. Bass, *Acta Cryst.*, 1987, C43, 1668-1674.
27. C.C. Stoumpos, C.D. Malliakas, and M. G. Kanatzidis, *Inorg. Chem.*, 2013, **52**, 9019-9038.
28. S. Ha, X. Liu, Q. Zhang, D. Giovanni, T. C. Sum and Q. Xiong, *Adv. Opt Mater.*, 2014, **2**, 838-844.
29. I. Borriello, G. Cantele, and D. Ninno, *Phys. Rev. B.*, 2008, **77**, 235214-4.
30. Q. Chen, H. Zhou, T. Song, S. Luo, Z. Hong, H. Duan, L. Dou, Y. Liu, Y. Yang, Controllable self-Induced passivation of hybrid lead Iodide perovskites toward high performance solar cells, *Nano Lett.*, 2014, **14**, 4158-4163.
31. C. -H. Chung, B. Bob, T. -B. Song, Y. Yang, *Sol. Energy Mater. Sol. Cells*, 2014, **120**, 642-646.
32. T. Supasai, N. Rujisamphan, K. Ullrich, A. Chemseddine, and Th. Dittrich, *Appl. Phys. Lett.*, 2013, **103**, 183906-3.
33. P. Pistor, J. Borchert, W. Fränzel, R. Csuk, R. Scheer, *J. Phys. Chem. Lett.*, 2014, **5**, 3308-3312.
34. A. Dualeh, N. Tétreault, T. Moehl, P. Gao, M. K. Nazeeruddin, M. Grätzel, *Adv. Funct. Mater.*, 2014, **24**, 3250-3258.
35. R. Lindblad, D. Bi, B. Park, J. Oscarsson, M. Gorgoi, H. Siegbahn, M. Odellius, E. M. J. Johansson, H. Rensmo, *J. Phys. Chem. Lett.*, 2014, **5**, 648-653.
36. V. G. Pedro, E. J. Perez, W. S. Arsyad, E. M. Barea, F. F. Santiago, I. M. Sero, and J. Bisquert, *Nano Lett.*, 2014, **14**, 888-893.
37. A. K. Chandiran, A. Yella, M. T. Mayer, P. Gao, M. K. Nazeeruddin, and M. Grätzel, *Adv. Mater.*, 2014, **26**, 4309-4312.
38. W. Liu, and Y. Zhang, *J. Mater. Chem. A*, 2014, **2**, 10244-10249.
39. T. Baikie, Y. Fang, J. M. Kadro, M. Schreyer, F. Wei, S. G. Mhaisalkar, M. Graetzel and T. J. White, *J. Mater. Chem. A*, 2013, **1**, 5628-5641.
40. W. A. Laban, and L. Etgar, *Energy Environ. Sci.*, 2013, **6**, 3249-3253.

Table of Content (TOC):**Text:**

A simple ITCVD method is developed to fabricate PSCs, and its roll over phenomenon in J-V curve is first investigated.